http://dx.doi.org/10.1080/14786435.2014.910333

Atomistic modelling of hydrogen segregation to the Σ9{2 2 1}[1 1 0] symmetric tilt grain boundary in Al

X.J. Shen[ab], D. Tanguy[a*] and D. Connétable[c]

[a] *Institut Lumière Matière, UMR5306 Université Lyon 1 – CNRS, Université de Lyon, 69622 Villeurbanne cedex, France;* [b] *State Key Laboratory of Molecular Reaction Dynamics and Center for Theoretical Computational Chemistry, Dalian Institute of Chemical Physics, Chinese Academy of Sciences, Dalian 116023, People's Republic of China;* [c] *CIRIMAT UMR 5085, CNRS-INPT-UPS, École Nationale d'Ingénieurs en Arts Chimiques et Technologiques (ENSIACET) 4, allée Émile Monso, BP 44362, F-31030 Toulouse Cedex 4, France*

The paper establishes a quantitative link between the bulk hydrogen content and the local concentration in the core of the Σ9{2 2 1}[1 1 0] symmetric tilt grain boundary in Al. A detailed map of *approximate* segregation energies is obtained by combined semi-empirical and *ab initio* calculations. Even if the density of trap sites and the binding to the core are large, it is shown that segregation alone is not expected to lead to a significant loss of cohesion below 1000 ppm bulk concentration. Other mechanisms should be involved, like H-induced structural changes, to explain the experimentally observed failure of the interfaces at low H concentration. An example of such mechanism is reported.

Keywords: *ab initio*; brittleness; grain boundary structure; hydrogen in metals

1. Introduction

Understanding hydrogen (H) embrittlement of metallic alloys is of great practical importance since it is often involved in critical damaging modes like stress corrosion cracking and corrosion fatigue [1]. The variety and intermixing of phenomena (surface reactivity, microstructure interplay with plasticity and diffusion) have made the analysis of experiments difficult [2], at a microscopic scale. In particular, a consensus on the physical origin of H induced fracture is not reached yet, with three main models proposed: decohesion, enhanced localized plasticity [3] and enhanced dislocation emission and nano-scale bubbles growth [4]. A critical review of decohesion can be found in [5].

It is useful to remind some essential experimental findings regarding intergranular H diffusion and fracture. Permeation experiments, with H generated from electrolytes, are used for studying diffusion under the influence of lattice defects like dislocations [6], grain boundaries of different nature [7] or vacancies coming from anodic dissolution at the surface [8]. In principle [9], it can be used to measure effective diffusion coefficients, bulk concentrations, and trapped hydrogen concentrations. The effective diffusion coefficient can be related to grain boundary segregation energies [10]. This is valid when trapping

*Corresponding author. Email: dome.tanguy@univ-lyon1.fr

dominates [11], but, in general, trapping and fast diffusion paths can be in competition. It was demonstrated recently, by *ab initio* calculations in Fe [12], that even in the case of simple GBs many different situations occur: $\Sigma 3$ and $\Sigma 5$ GBs in bcc Fe trap and slow down diffusion while, in fcc Fe, the $\Sigma 3$ GB repels H and the $\Sigma 11$ traps H and offers an easy diffusion path parallel to the GB plane. In this case, a concentration dependence is expected with slow diffusion at low concentration and the activation of easy diffusion path when the deep traps are saturated. This kind of complexity should be included in physical models of effective diffusion coefficients [13]. Building reliable, GB specific, segregation energy maps is a necessary step is this direction.

Concerning the fracture aspect, several *ab initio* studies deal with the impact of segregations on the ideal work of fracture [14–17]. It should be recalled that, in the case of hydrogen, embrittlement is not straightforwardly related to H segregation. Experiments show that crack *propagation* along the GBs is often strain rate dependent, i.e. at high strain rate fracture is ductile, even in the presence of internal hydrogen [18–20]. H segregation alone is not enough to induce fracture at the concentration levels considered in these experiments. On the contrary, crack *initiation* from a flat surface exposed to severe H uptake conditions can proceed by decohesion at low average stress levels [21]. From this brief overview, we can conclude that knowing the relation between average bulk concentrations, that can be measured experimentally, and local intergranular concentrations, that cannot be measured experimentally, would constitute a very valuable information when trying to establish microscopic fracture models. Establishing such relation, from predictive atomic scale simulations, is precisely the goal of the present paper.

Semi-empirical and *ab initio* calculations are combined to study in detail the $\Sigma 9\{2\,2\,1\}$ [1 1 0] symmetric tilt grain boundary. Although specific to this GB, the results can be extended to the whole family of GBs having the same tilt axis following the structural unit model. Aluminium is chosen as a archetype of face-centred cubic materials. It has the interesting property that point defect formation energy is low and H segregation to defects is strong. It is therefore prone to H-induced structural modifications, as will be shown.

The paper is organized as follows: First, methods and the construction of the grain boundary are described. Second, *approximate* hydrogen segregation energies are given, with an emphasis on quantum corrections. Local concentrations are calculated in the mean field approximation. It is shown that the density of deep trap sites is such that H–H interactions play a crucial role. Finally, the influence on fracture is discussed and perspectives are given.

2. Methods

Searching for metastable grain boundary structures and calculating segregation energies are computationally intensive tasks. Therefore, the work is divided in two parts. First, a systematic search of local energy minima is made with an empirical interatomic potential. Second, the most relevant configurations are selected and re-converged by an *ab initio*, more predictive, method. Finally, the local concentrations in the GB, as a function of thermodynamic parameters, are obtained by mean field equations.

2.1. *Empirical potential and grain boundary structure*

In a first step, interatomic forces are modelled by the Mishin embedded atom method (EAM) potential for Al [22]. The GB structure searches consist in: (i) Constructing an initial

geometric structure based on the coincidence site lattice (CSL). (ii) Exploring the stability of the various structures obtained by translating one grain with respect to the other. (iii) Optimizing the number of the particles in the interface. The unit cell of the CSL corresponding to the symmetrical $\Sigma 9\{2\,2\,1\}[1\,1\,0]$ GB is shown in Figure 1. Only translations in the X and Y directions are explored and the size of the CSL gives an upper bound for the amount of translation to be applied. A 5×10 grid of points was therefore generated with steps $0.1\,a_0$ in the X direction and $0.21\,a_0$ in the Y direction. The simulation box for EAM calculations contains 5136 particles (4 CSL in the Y direction, 12 CSL in the Z direction). Minimizations are done using molecular dynamics and a 'quench' condition that is: setting all velocities of relaxed atoms to zero when $\sum_i \vec{v}_i \cdot \vec{f}_i < 0$.

The atoms belonging to the border of the slab in the X direction are kept fixed, while the atoms whose positions are less than $5\,a_0$ are allowed to relax. Periodic boundary conditions are applied in the Y and Z directions. The total potential energy of the GB structure is converged within 0.1 meV and the averaged force of each relaxed atom is less than 0.5 meV/Å.

The Al–H interactions are also modelled within the EAM framework. While the Al–Al part is the Mishin potential, the Al–H part is an upgrade of the potential presented in [23]. The parameters for the functional forms are given in Appendix 1.

The initial configurations for hydrogen segregation in the grain boundary are geometrically constructed as if the metal atoms of the GB were bulk atoms, i.e. for each bulk atom, there are one octahedral and two tetrahedral sites, constructed by displacements relative to the metal site. By doing so, and taking into account the mirror symmetry of the GB, the system is continuously and densely paved with interstitial sites. In the GB region, 57 initial configurations are constructed and relaxed with EAM. Some of these configurations lead to the same local minimum energies.

2.2. *Density functional theory calculations*

In order to obtain reliable equilibrium structures of GBs and segregation energies, we perform energy optimizations by *ab initio* calculations. They are based on density functional theory (DFT) and carried out with the generalized gradient approximations to the exchange-correlation functional (Perdew–Burke–Ernzerhof) [24], as implemented in the Vienna *Ab initio* Simulation Package [25]. We use projector augmented wave [26] method for valence electrons and a $1 \times 5 \times 5$ k-points grid for the Brillouin zone sampling. Plane waves are used for expanding the wave functions with a cut-off energy equal to 400 eV. A supercell approach is adopted which includes 104 metal atoms for each grain boundary structure. It contains one CSL unit in the Y direction and two in the Z direction, while in the X direction, each border is a free surface with 11 rigid atomic layers and a 7.0 Å wide vacuum space between periodic images. Relaxations are carried out until the force is less than 0.01 eV/Å. Every segregation energy includes a zero point vibrational energy correction. It is estimated from a dynamical matrix corresponding to the degrees of freedom of hydrogen only, using the frozen phonon approach (the relative displacements are equal to 0.01 Å) [27,28].

2.3. *Approximate segregation energies and mean field equations*

We can build a free energy functional which on optimization gives the mean occupancy of the interstitial sites of the GBs. An approximate mean internal energy is obtained from the

segregation energies defined on each interstitial site (i) of the GB (ΔE^i_{seg}). The 'true' segregation energy is obtained by taking the difference in potential energy between a configuration, where H is placed on site i and a configuration where H is in the bulk, at zero K (the energy is at its minimum), in the infinite dilution limit. In practice, the system is small and therefore only approximate values can be obtained because of H interactions between periodic images and 'bulk' H interactions with the GB. In the perfect crystal case, the size dependence of the immersion energy is tested in [27] and seems to be well converged beyond 32 atoms within a few tens of meV. In our case, the 'bulk' site (site H_1 on Figure 1) is inside a box containing a GB. It should not be too close to the GB and not too close to the rigid border. The deviation in energy of this configuration from the 'true' bulk case (which would be the well-converged isolated H in the perfect crystal) is quantified by calculating the difference in embedding energy with a perfect crystal containing 108 atoms ($3 \times 3 \times 3$ unit cells), the maximum size in [27]. It is 40 meV. Therefore, our *approximate* segregation energies differ only by a few tens of meV from the 'true' segregation energies, slightly below the intrinsic difference between DFT and experiments for the immersion energy and diffusion barrier [27]. Throughout the text, the 'segregation energy' (ΔE^i_{seg}) should be understood as the *approximate* segregation energy, as defined in this section.

As will appear clearly below, the specificity of the GB core requires that the H–H interactions be included. This is done by calculating effective pair interactions (ϵ_{ij}). They are calculated by taking the energy difference between two configurations containing two hydrogen atoms: the final one where the two H atoms are close and the reference one where each solute is on its GB site but far enough so that the interaction between them can be neglected. In DFT, the system size is such that the calculation is done in a different way: the reference energy (E'_{ref}) corresponds to a configuration with one H atom on its GB site (for example site j) and the second one on a bulk site. Then, using the value of the segregation energy on site i, the effective pair interaction ϵ_{ij} between site i and j is :

$$\epsilon_{ij} = E_{ij} - (E'_{ref} + \Delta E^i_{seg}) \tag{1}$$

where E_{ij} is the energy of the configuration where the sites i and j are occupied.

The free energy as a function of the average occupancies of sites c_i (that include GB and bulk sites c_{bulk}) is:

$$F_{N_H,V,T}(\{c_i\}) = E_0 + \sum_i \left\{ c_i \Delta E^i_{seg} + \sum_j c_i c_j \epsilon_{ij} + kT \left(c_i \ln c_i + (1 - c_i) \ln(1 - c_i) \right) \right\} \tag{2}$$

The constraint of a fixed number of H atoms N_H is taken into account by introducing a Lagrange multiplier μ_H. Writing the optimization condition for each kind of site, one obtains:

$$\begin{aligned} \frac{c_i}{1 - c_i} &= e^{-(\Delta E^i_{seg} + \sum_j c_j \epsilon_{ij} - \mu_H)/kT} \\ \frac{c_{bulk}}{1 - c_{bulk}} &= e^{\mu_H / kT} \end{aligned} \tag{3}$$

The equations, and approximations, specific to the GB structure are given in Section 3.3. To be coherent with this model, the concentrations mentioned in the paper are the mean

occupancies. In particular c_{bulk} is the mean occupancy of a bulk tetrahedral site (there are two T sites per metal atom).

3. Results

3.1. *Atomic structure of the* $\Sigma 9\{2\,2\,1\}[1\,1\,0]$ *grain boundary in Al*

Two stable structures are found. The first one (GB1) is composed of two 'E' structural units [29,30] (Figure 1), the second one (GB2) is mirror symmetric with respect to the GB plane (Figure 2). Both have been observed experimentally using high resolution TEM [31]. The structures we find are in good agreement with those obtained from previous calculations based on EAM potentials for metals [29,30]. They are connected by a translation along the Y axis ($t_y \approx -0.212\,a_0$, plus a shift of the GB plane to the right side of the box, by one plane). The interface excess energies, from EAM calculations, are 455 and 485 mJ/m^2 for 'E-units' (GB1) and 'mirror symmetry' (GB2) boundaries, respectively, which are in good agreement with the values at $T = 300$ K reported [30] (435 and 468 mJ/m^2). Furthermore, DFT calculations give an energy difference of 64.6 mJ/m^2 between these two structures.

3.2. *Approximate hydrogen segregation energies*

Calculating H segregation energies requires a reference configuration which is obtained by placing the solute as far from the GB as possible. Next, a series of calculations on configurations where the solute is placed at different locations in the GB are done. The segregation energy ΔE^i_{seg} is the difference between this configuration's energy and the reference's (with the precautions exposed in Section 2.3). Therefore, a negative ΔE^i_{seg} (resp. positive) value means an enrichment (resp. depletion) with respect to the bulk. In Section 2, we explained how the interstitial sites for hydrogen are geometrically constructed. Starting from there, a first energy minimization is done with the EAM potential and the relaxed configuration is passed to DFT for a second energy minimization. All the possible final

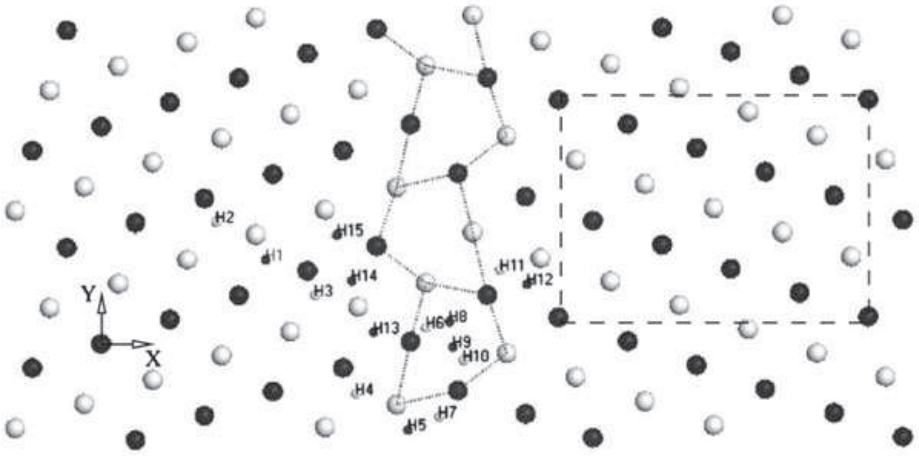

Figure 1. Atomic structure of the $\Sigma 9\{2\,2\,1\}[1\,1\,0]$ symmetric grain boundary after relaxation with DFT. Black and white balls represent two $\{2\,2\,0\}$ planes. The small balls represent stable interstitial positions for isolated H atoms. Site labels are coherent throughout the paper. The 'E' structural units are underlined, as well as a CSL unit cell. This structure is referred to as GB1.

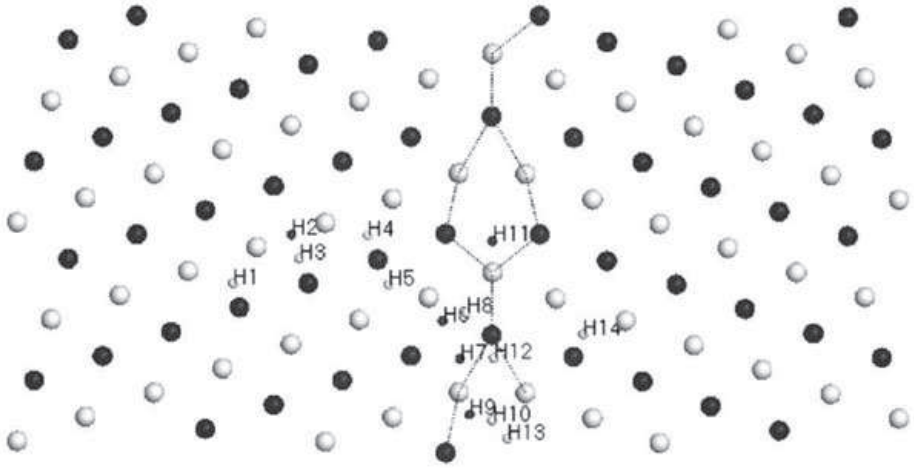

Figure 2. 'Mirror symmetric' (GB2) atomic structure of the $\Sigma 9\langle 1\,1\,0\rangle\{2\,2\,1\}$ symmetric grain boundary after relaxation with DFT.

hydrogen positions are represented in Figures 1 and 2. The corresponding segregation energies are given in Tables 1 and 2, which include positions and energies obtained by DFT, with and without the zero point energy (ZPE) corrections. The values from EAM are also shown. The quality of the EAM potential is discussed in Appendix 1. Some values are clearly smaller than the 'error' of 40 meV discussed in Section 2.3, and therefore should not be considered as corresponding to enrichment or depletion sites. They are in the tables to give the reader a feeling of the variability of the energy landscape when choosing the 'bulk' site for the segregation energy calculation.

In bulk Al, hydrogen on octahedral and tetrahedral sites give very similar energies, with a slight preference for the tetrahedral site (40 meV, including ZPE [27]). The ZPE of hydrogen is very significant and reduces the energy difference by about 100 meV [27]. In the grain boundary, the most stable positions are also those obtained by relaxation from tetrahedral positions. GB1 and GB2 have similar hydrogen segregation energies. The contributions of the ZPE to ΔE^i_{seg} are large: down to -50 meV (resp. -100 meV) for the 'E units' of GB1 (resp. GB2). The influence of the GBs is short range: beyond $1.5\,a_0$, $|\Delta E^i_{seg}|$ falls below 0.05 eV. The 'E-unit' core contains a cluster of favourable sites (labelled H8, H9 and H10). On site 9, for example, ΔE^i_{seg} is as low as -0.357 eV (the three vibrational frequencies of hydrogen are 136, 107 and 37 cm^{-1}), very close to the one in vacancies (-0.33 eV [27]). Besides the core (sites 11–15), the segregation energies are significant but much higher (of the order of -0.1 eV).

In GB2, the situation is more complex. The core sites 9, 10 and 13 have ΔE^i_{seg} values close to the value in the vacancy. The other structural unit, which is more 'twin like', also show values of the same order of magnitude (Table 2 for sites 6–8 in Figure 2). It is surprising since a twin is not a strong trap [12]. The analysis of the Al positions, after hydrogen relaxation, reveals H *induced structure changes* (Figure 3). Only a few local distortions are necessary to switch from the twin unit to the E-unit and, after relaxation, the hydrogen atom is in an environment that resembles the one in the core of the E-unit. Energetically, there are several contributions to ΔE^i_{seg} on these sites: the decrease in the energy due to the occupancy of a newly formed core-like interstitial sites (-0.3 eV), the transformation from GB2 to GB1 (-0.102 eV per structural unit) and the interface excess

Table 1. Positions (in a_0) and *approximate* segregation energies ΔE^i_{seg} (in eV) obtained by energy minimization with EAM and DFT for the 'E-units' structure (GB1). ΔE^{iZPE}_{seg} (in eV) is the segregation energy including the ZPE correction. The site numbers (i) refers to Figure 1. ϵ_{9-i} (in eV) is the pair interaction energy between site number 9 and its neighbours. The asterisk marks those obtained in the infinite dilution limit, the others correspond to a saturated line of sites 9.

	EAM				DFT					
Site i	x	y	z	ΔE^i_{seg} (eV)	x	y	z	ΔE^i_{seg}	ΔE^{iZPE}_{seg}	ϵ_{9-i}
1	−1.818	1.778	0.000	−0.002	−1.805	1.771	0.000	0.000	0.000	0.000
2	−2.323	0.010	0.354	−0.002	−2.294	0.015	0.354	0.042	0.046	0.000
3	−1.317	1.423	0.354	0.008	−1.324	1.421	0.354	0.016	0.019	0.000
4	−0.956	0.481	0.354	−0.047	−0.922	0.455	0.354	−0.083	−0.103	0.130
5	−0.486	0.133	0.000	−0.201	−0.416	0.104	0.000	−0.277	−0.297	–
6	−0.280	1.134	0.354	−0.166	−0.117	1.084	0.354	−0.135	−0.180	0.041*
7	−0.070	0.251	0.354	−0.205	−0.109	0.232	0.354	−0.204	−0.245	–
8	−0.101	1.320	0.000	−0.209	−0.058	1.289	0.000	−0.235	−0.275	0.070*
9	−0.048	0.865	0.000	−0.191	*0.024*	*0.915*	*0.000*	*−0.338*	*−0.357*	–
10	0.183	0.744	0.354	−0.150	0.127	0.785	0.354	−0.258	−0.279	0.011*
11	0.423	1.657	0.354	−0.010	0.485	1.671	0.354	−0.077	−0.095	0.100
12	0.791	1.556	0.000	−0.041	0.752	1.533	0.000	−0.100	−0.118	0.174
13	−0.811	1.061	0.000	0.002	−0.751	1.061	0.000	−0.090	−0.103	0.052
14	−0.985	1.549	0.000	0.015	−0.964	1.564	0.000	−0.061	−0.064	0.000
15	−1.140	2.023	0.000	−0.004	−1.108	2.009	0.000	−0.057	−0.066	−0.014

*infinite dilution limit.

energy when a mixture of GB1 and GB2 domains exists in the GB plane. Elastic distortions in the grain neighbourhood are also present. Indeed, a complete transformation requires a shift in the Y direction, while such translation is constrained in the DFT calculation. As a consequence, it exists a strain field (mostly shear strain ϵ_{xy}) beside the GB, and the current calculation would give a size dependence of the segregation energy. Nevertheless, the *ab initio* calculation shows there exist a driving force for H-induced local structure changes. They have important consequences: they change the density and depth of traps along the GB, key factors in the loss of intergranular cohesion.

The essential findings in this section are: First, we found a mechanism for increasing the density of deep trap sites in the GB2 unit that consists in a local change from GB2 towards GB1. Second, GB1 has a core that acts as a strong trap for H. But, the core sites 8, 9 and 10 are very close one to the other ($d_{9-8} \approx 0.47$ and $d_{9-10} \approx 0.52\,a_0$) so the question of the short-range interaction between H impurities has to be investigated. In the next section, we address this point, together with the average occupancy of these sites as a function of the bulk concentration and temperature. The effective density of trap sites is also discussed.

3.3. *Grain boundary mean occupation by hydrogen, as a function of T and C_{bulk}*

In this section, the focus is on GB1 only, since GB2 has a tendency to be destabilized in case of H segregation. In GB1, site 9 has the lowest segregation energy, followed by sites 8 and 10. In case of an increase of the bulk H content (like the passage of a hydrogen

Table 2. Positions (in a_0) and *approximate* segregation energies ΔE^i_{seg} (in eV) obtained by energy minimization with EAM and DFT for the 'mirror symmetry' structure (GB2). ΔE^{iZPE}_{seg} (in eV) is the segregation energy including the ZPE correction. The site numbers refer to Figure 2. The † symbol means that H-induced a structure change of the GB.

	EAM				DFT				
Site i	x	y	z	ΔE^i_{seg}	x	y	z	ΔE^i_{seg}	ΔE^{iZPE}_{seg}
1	−2.200	1.645	0.354	0.000	−2.178	1.644	0.354	0.000	0.000
2	−1.610	2.114	0.000	0.139	−1.612	2.116	0.000	0.063	−0.036
3	−1.533	1.879	0.354	−0.004	−1.538	1.886	0.354	0.016	0.011
4	−0.868	2.102	0.354	−0.012	−0.875	2.108	0.354	−0.042	−0.045
5	−0.687	1.641	0.354	−0.035	−0.674	1.628	0.354	−0.065	−0.082
6	−0.209	1.288	0.000	−0.133	−0.150	1.279	0.000	−0.292	−0.326 †
7	−0.001	0.857	0.000	−0.127	0.017	0.911	0.000	−0.264	−0.320 †
8	0.077	1.352	0.354	−0.166	0.076	1.358	0.354	−0.262	−0.309 †
9	0.205	0.347	0.000	−0.174	0.146	0.339	0.000	−0.317	−0.352
10	0.331	0.416	0.354	−0.205	*0.329*	*0.315*	*0.354*	*−0.328*	*−0.360*
11	0.331	2.010	0.000	−0.224	0.332	2.052	0.000	−0.242	−0.294
12	0.331	0.900	0.354	−0.191	0.346	0.920	0.354	−0.095	−0.136
13	0.619	0.165	0.354	−0.162	0.478	0.137	0.354	−0.203	−0.299
14	1.145	1.159	0.354	−0.019	1.213	1.149	0.354	0.005	0.001

† H-induced a structure change of the GB.

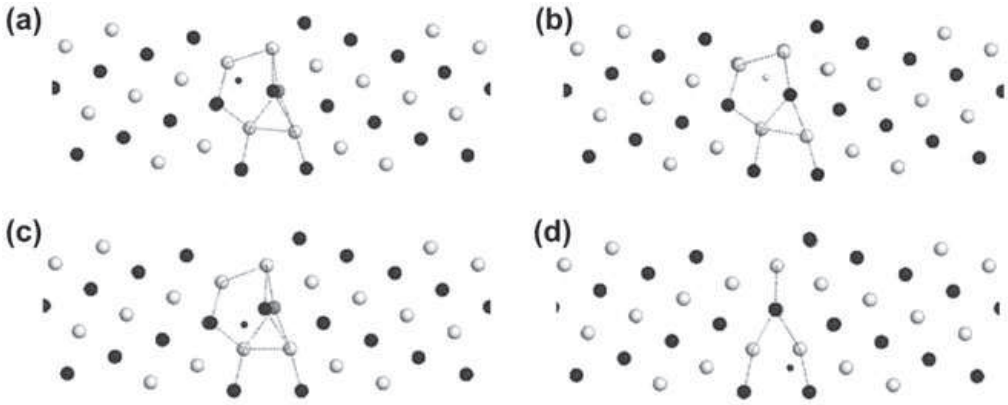

Figure 3. H influence on the GB2 structure: different pictures correspond to different initial positions of H in the GB2 structure (a) position 6, (b) position 8, (c) position 7 and (d) position 9.

diffusion front), site 9 is saturated first. It is therefore natural to calculate the effective pair interaction between site 9 and site 8, and between site 9 and site 10. Their values are given in Table 1. The three-body interaction is negligible (lower than 10 meV). Then, the specific segregation isotherms, to be solved numerically, are:

$$\frac{c_9}{1-c_9} = e^{(-(\Delta E^9_{seg} + c_8\,\epsilon_{9-8} + 2c_{10}\,\epsilon_{9-10} - \mu_H)/kT)}$$

$$\frac{c_8}{1-c_8} = e^{(-(\Delta E^8_{seg} + c_9\,\epsilon_{9-8} - \mu_H)/kT)}$$

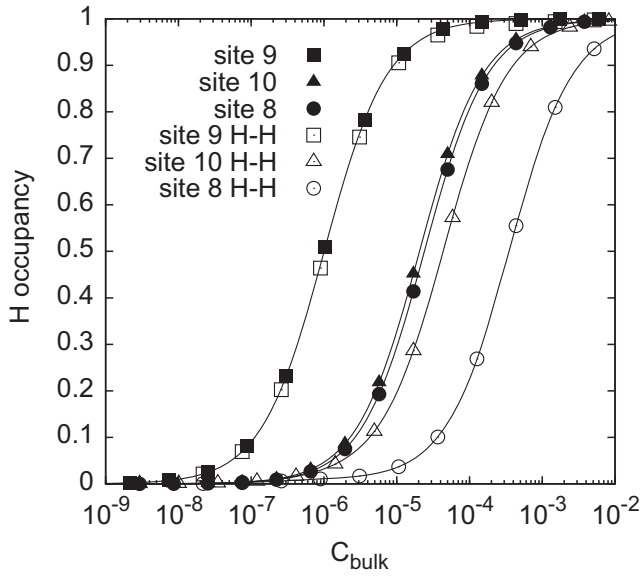

Figure 4. Bulk concentration dependence of the mean occupancy of sites 9, 8 and 10 in GB1, at $T = 300$ K without (black symbols) and with the H–H interactions (white symbols). The very high bulk concentrations (mean tetrahedral site occupancy) correspond to hypothetical metastable solid solutions. Which phase or defects are created at high concentrations is not clear and depends on kinetics [32].

$$\frac{c_{10}}{1-c_{10}} = e^{(-(\Delta E^{10}_{seg} + 2c_9\,\epsilon_{9-10} - \mu_H)/kT)}$$
$$\frac{c_{bulk}}{1-c_{bulk}} = e^{\mu_H/kT} \tag{4}$$

where c_9, c_8 and c_{10} are the average occupancies of sites 9, 8 and 10. Note that the factor 2 in front of ϵ_{9-10} is a geometric factor that comes from the fact that the solutes are located in different {2 2 0} planes and therefore one site of type 9 can be connected to two sites of type 10. The numerical results are shown in Figure 4.

At $T = 300$ K, site 9 starts to be occupied at very low bulk concentration. The occupancy is 10% at about 10^{-7} atomic concentration in the bulk. The influence of the H–H interactions is negligible because sites 8 and 10 start being occupied at concentrations where 9 is already almost saturated. On the opposite, the influence of 9 on sites 10 and 8 is large. Their occupancies are shifted towards higher concentrations by, respectively, a factor of 2 and a factor of 20. This means that while site 9 is saturated at about 10^{-5} (occupancy reaches 90%), site 8 is saturated at 3×10^{-3} and site 10 at 4×10^{-4}. 5×10^{-4} is already an upper limit for mobile H concentrations in Al [33]. At this concentration, there should be two H atoms per E-unit.

The others sites have segregation energies higher than -0.12 eV. Their concentration reaches 10% only beyond 1000 ppm. It has been recently proposed that high local concentrations can act as a seed for local hydrides in Ni [34,35] because of the attractive H–H interactions ($\epsilon_{\mathrm{H-H}} \approx 20$ meV). Even though the hydride is unstable with respect to hydrogen gas at room temperature [36] in Al, it is interesting to calculate the pair interactions, close to the GB, when the concentration is high in the core. We simplify the configurations described above by saturating only site 9. Then, the pair interactions are calculated for sites 4, 11–15 (Table 1). The repulsion is usually strong, except on site 15. No enhanced hydrogen

segregation in the first planes close to the core is to be expected in this GB due to the H–H interactions. The stability of the H_2 molecule in the core of the E unit was also studied. It was found that wherever the molecule is inserted, it always dissociates.

4. Discussion

What is the impact of this segregation on the cohesion of the grain boundary? As a first approach, we can calculate the ideal work of fracture as a function of c_{bulk}. It is important to clearly state the hypothesis that is made. The initial configuration is a GB in equilibrium with the bulk at a concentration c_{bulk} and temperature T. The grain boundary structure is the GB1 given in Figure 1, which gives a specific density of trap sites (a number of sites per surface unit). From the mean field analysis, we learn that the occupied sites, in the concentration range 10–1000 ppm, are sites 9, 10 and 8 and that the repulsive interactions between them are important. The density of such sites (labelled θ) is 2/A, where $A = \delta Y \times \delta Z$ ($\delta Y = 2\,a_0$, $\delta Z = \sqrt{2}/2\,a_0$) is the surface of one CSL unit. Each site has a specific segregation energy that depends on the occupation of the others sites (Equation (4)). Then, the final, broken, configuration is the one where the crack plane is the GB plane and two surfaces of {2 2 1} type are created. We idealize fracture by considering that only hydrogen atoms that are present in the GB sites 8, 9 and 10 are present on the newly created surfaces. It is a hypothetical, instantaneous and brittle fracture. H atoms on the surface are relaxed. The {2 2 1} surfaces are composed of {1 1 1} terraces and steps. It is reasonable to approximate the hydrogen segregation energy to the surface by the value for the {1 1 1} surface [37]: −0.38 eV/H. The ideal work of separation is

$$\begin{aligned} W_{sep}(c_{bulk}) &= (E_{surf} - E_{GB})/A \\ &= 2\left(\gamma_S + \theta_S c_S(c_{bulk})\Delta E_{seg}^{surf}\right) \\ &\quad - \left(\gamma_{GB} + \sum_i \theta_{GB}^i c_i(c_{bulk})\Delta E_{seg}^i\right) \\ &= 2\gamma_S - \gamma_{GB} \\ &\quad + \sum_i \theta_{GB}^i c_i(c_{bulk})(\Delta E_{surf} - \Delta E_{seg}^i) \end{aligned} \tag{5}$$

where we made use of $2\theta_S c_S(c_{bulk}) = \sum_i \theta_{GB}^i c_i(c_{bulk})$ since no diffusion occurs during fracture. The work of fracture in the absence of hydrogen is $2\gamma_S - \gamma_{GB}$ where γ_S is the surface energy and γ_{GB} is the grain boundary excess energy. The value for ideal work without hydrogen is 1.555 J/m^2 from [38]. The sum runs over sites 8, 9 and 10 and θ_{GB}^i is constant and equal to $4/3\,a_0^2$ as discussed above. The occupancies $c_i(c_{bulk})$ are given, at $T = 300$ K, by the mean field equations. The site specific segregation energies are given in the exponential of Equation (4). The numerical results are shown in Table 3 where the contribution of each site is given separately for three different bulk concentrations. It is interesting to realize that the influence of the sites that are weak traps becomes dominant when the bulk concentration increases.

The model gives a decrease of the work of separation of, at most, 25%. We believe that in order to have a crack that follows the core of a grain boundary, dislocation emission from the crack tip itself should be severely reduced (which does not mean that the neighbouring matrix cannot deform plastically due to the activity of external dislocation sources). The

Table 3. Influence of the H segregation on the ideal work of separation (ΔW_{sep}). $W^0_{sep} = 1.555\,\mathrm{J/m^2}$ is the ideal work of fracture without H [38].

Site i	c_{bulk}	ΔW_{sep} J/m^2	$W_{sep}(c_{bulk})/W^0_{sep}$ (%)
	10^{-5}	−0.078	95
9		60%	
10		40%	
8		0%	
	10^{-4}	−0.225	85
9		23%	
10		49%	
8		28%	
	10^{-3}	−0.391	75
9		13%	
10		38%	
8		49%	

simulation of the critical stress intensity factor (K) for dislocation emission gives values that are of the order of 70% of the Griffith value, in {1 1 1} [39,40] single crystals. As the Griffith K scales with the square root of the ideal work of separation (for an idealized planar crack propagation), getting enough 'embrittlement' to fall below 70% K would require a drop of W_{sep} by approximately 50%. This is twice the value we obtain. In the $\Sigma 5\{2\,1\,0\}[1\,0\,0]$ symmetrical grain boundary, comparable segregation energies (−0.25 eV/H) are reported in [41], but much lower value was taken for the segregation to the surface (−0.75 eV/H), which gives a much larger impact on the work of separation. The reduction can go down to 90%. In our case, we consider the segregation on a {1 1 1} surface instead of a {2 1 0} surface. It is shown in [42] that H has the strong binding to steps on {1 1 1} surfaces, up to 0.2 eV, which in this case brings the value (−0.38 to 0.2) closer to the one reported in [41]. Finally, these considerations bring us back to the core of the fracture problem: the crack path can have a nanoscale rugosity, in relation with the preferential segregation of H on surfaces. Such effects are not included in the fracture criterion discussed here. Nevertheless, our calculation points out that, even if embrittlement could be effective with an enhanced segregation on steps, it would happen for bulk concentrations of the order of 1000 ppm and beyond.

5. Conclusion

We report *approximate* hydrogen segregation energy maps for the two most stable structures of $\Sigma 9\{2\,2\,1\}[1\,1\,0]$ symmetrical grain boundary in Al. The core of the E structural unit offers a large density of trap sites, with energies of the order of −0.3 eV/at, including non negligible ZPE corrections. In the case of the symmetrical structure (GB2), the 'twin' like units are found to be unstable upon H segregation. H triggers local distortions to transform GB2 into GB1. This gives an interesting mechanism where interfaces of slightly higher energy than

the optimum have more flexibility to rearrange and offer favourable local environments for H. The result is an enhanced intergranular concentration via an increase in the density of trap sites, that in turns can favour decohesion. mean field equations, including H–H repulsion in the core of the E unit, are used to evaluate the local concentration inside GB1 as a function of the bulk concentration at $T = 300$ K. It is found that the core sites are being enriched at 0.1 ppm and saturate at 1000 ppm. The corresponding high local concentration does not act as a seed for a local hydride, as reported in the literature for Ni. Finally, the impact of such segregation on the ideal work of fracture is discussed. This GB could be embrittled by H segregation alone, but only at bulk concentrations beyond 1000 ppm. This means that other mechanisms than a simple segregation should be involved when crack propagation is observed below 1000 ppm. Future work will be devoted to the study of GB structure modifications induced by massive hydrogen segregation and their consequences on mechanical properties. The idea is to investigate the kind of structural rearrangements that we observed here by DFT but in a more systematic way by Monte Carlo simulations and the well-tested EAM potential described in Appendix 1.

Funding

This work is supported by the French Agence Nationale de la Recherche (ANR) under grant *EcHyDNA* (Blanc 1019424). This work was granted access to the HPC resources of CALMIP (CICT Toulouse, France) under the allocation 2013-p0749 and PSMN at the ENS de Lyon. CNRS (INP) is also gratefully acknowledged for additional funding.

References

[1] T. Magnin, *Second International Conference on Corrosion Deformation Interactions*, The Institute of Materials, Nice, 1997.
[2] N.J.H. Holroyd, *Environment-Induced Cracking of High-Strength Aluminum Alloys*, in *EICM Proceedings*, R.P. Gangloff and M.B. Ives, eds. *Environment-Induced Cracking of Metals*, NACE, Houston, Tx, 1990, p.311.
[3] P. Sofronis and H. Birnbaum, J. Mech. Phys. Solids 43 (1996) p.49.
[4] S. Lynch, Acta Metall. 36 (1988) p.2639.
[5] H. Birnbaum, I. Robertson, P. Sofornis and D. Teter, *Mechanisms of Hydrogen Related Fracture-a review*, in *Second International Conference on Corrosion Deformation Interactions*, T. Magnin, ed., The Institute of Materials, 1997, p.172.
[6] A.M. Brass and A. Chanfreau, Acta Mater. 44 (1996) p.3823.
[7] A. Oudriss, J. Creus, J. Bouhattate, E. Conforto, C. Berziou, C. Savall and X. Feaugas, Acta Mater. 60 (2012) p.6814.
[8] J. Ai and J.R. Scully, Corrosion 69 (2013) p.752.
[9] T. Zakroczymski, Electrochim. Acta 51 (2006) p.2261.
[10] R. Kirchheim and U. Stolz, J. Non-Cryst. Solids 70 (1985) p.323.
[11] T. Mütschele and R. Kirchheim, Scr. Metall. 21 (1987) p.135.
[12] Y.A. Du, L. Ismer, J. Rogal, T. Hickel, J. Neugebauer and R. Drautz, Phys. Rev. B 84 (2011) p.144121.
[13] Y.A. Du, J. Rogal and R. Drautz, Phys. Rev. B 86 (2012) p.174110.
[14] M. Yamaguchi, M. Shiga, and H. Kaburaki, Science. 309 (2005) p.1677d.
[15] S. Zhang, O.Y. Kontsevoi, A.J. Freeman and G.B. Olson, Appl. Phys. Lett. 100 (2012) p.231904.

[16] L. Zhong, R. Wu, A.J. Freeman and G.B. Olson, Phys. Rev. B 62 (2000) p.13938.
[17] P. Lejček, M. Šob, V. Paidar and V. Vitek, Scr. Mater. 68 (2013) p.547.
[18] N. Holroyd and D. Hardie, Corros. Sci. 21 (1981) p.129.
[19] N.B. Ali, R. Estevez and D. Tanguy, in *2012 International Conference on Effects of Hydrogen on Materials*, B. Sommerday and P. Sofronis, eds. ASME, Jackson Lake Lodge, Wyoming, 2014, pp. 697–705.
[20] J. Chene and A.M. Brass, Metall. Mater. Trans. A 35 (2004) p.457.
[21] E. Pouillier, A.F. Gourgues, D. Tanguy, and E.P. Busso, Int. J. Plast. 34 (2012) p.139.
[22] Y. Mishin, D. Farkas, M.J. Mehl and D.A. Papaconstantopoulos, Phys. Rev. B 59 (1999) p.3393.
[23] D. Tanguy and T. Magnin, Phil. Mag. 83 (2003) p.3995.
[24] J. Perdew, K. Burke and M. Ernzerhof, Phys. Rev. Lett. 77 (1996) p.3865.
[25] J. Kresse and J. Hafner, Phys. Rev. B 47 (1993) p.558.
[26] G. Kresse and D. Joubert, Phys. Rev. B 59 (1999) p.1758.
[27] C. Wolverton, V. Ozoliņš and M. Asta, Phys. Rev. B 69 (2004) p.144109.
[28] Y. Chen, C. Fu, K.-M. Ho and B. Harmon, Phys. Rev. B 31 (1985) p.6775.
[29] J.D. Rittner and D.N. Seidman, Phys. Rev. B 54 (1996) p.6999.
[30] L. Wan and S. Wang, Phys. Rev. B 82 (2010) p.214112.
[31] M.J. Mills, Mater. Sci. Eng. A 166 (1993) p.35.
[32] Y. Fukai, *The Metal-Hydrogen System: Basic Bulk Properties*. 2nd ed., Springer-Verlag, GmbH & Co. K, Berlin and Heidelberg, 2003.
[33] C. Buckley and H. Birnbaum, J. Alloys Comp. 330–332 (2002) p.649.
[34] J. Song, and W.A. Curtin, Acta Mater. 59 (2011) p.1557.
[35] J. von Pezold, L. Lymperakis and J. Neugebeauer, Acta Mater. 59 (2011) p.2969.
[36] G. Sinke, L. Walker, F. Oetting and D. Stull, J. Chem. Phys. 47 (1967) p.2759.
[37] D. Jiang and E. Carter, Acta Mater. 52 (2004) p.4801.
[38] X. Pang, N. Ahmed, R. Janisch and A. Hartmaier, J. Appl. Phys. 112 (2012) p.023503.
[39] D. Tanguy, Phys. Rev. B 76 (2007) p.144115.
[40] K. Gouriet and D. Tanguy, Phil. Mag. 92 (2012) p.1663.
[41] M. Yamaguchi, K. Ebihara, M. Itakura, T. Kadoyoshi, T. Suzudo and H. Kaburaki, Metall. Mater. Trans. A 42 (2011) p.330.
[42] R. Stumpf, Phys. Rev. Lett. 78 (1997) p.4454.
[43] D. Connétable, Y. Wang, and D. Tanguy, J. Alloy Compd. submitted (2014).

Appendix 1. EAM Al–H interactions

The model used for the Al–H interactions was first presented in [23]. The potential is designed to reach a compromise between the properties that we think are the most important for intergranular embrittlement, in particular, the segregation to vacancies. A practical issue is that we want an Al–H potential that is independent of the Al–Al part because we want to use it as an extension of already developed potentials without altering them. In the EAM framework, the total potential energy of the system has the form:

$$E_{pot} = \sum_i \left\{ F_I\left(\rho\left(\vec{r_i}\right)\right) + 1/2 \sum_{j \neq i} V_{IJ}\left(\|\vec{r_j} - \vec{r_i}\|\right) \right\} \tag{A1}$$

where the sum runs over the particles labeled i (or j, the neighbours of i). F_I is the embedding energy of a the particle i, which type is designated by I, and V_{IJ} is the type-dependent pair interaction between particles i and j. ρ is the electronic density, built by the surrounding, at the position where the particle is embedded. ρ is a sum of contributions from the neighbours $\rho(\vec{r_i}) = \sum_{j \neq i} \rho_{at}(\|\vec{r_j} - \vec{r_i}\|)$, but F_I is not linear and therefore, it is in general not possible to split the contribution coming from the H atoms from the one coming from the metal. We make the following 'approximation' that the electronic density contribution from H to the embedding density for the metal atoms is negligible

Table A1. Analytic forms for the embedding energy of H in Al. The electronic density is in arbitrary units, but in coherence with the function given in Table A2.

ρ	$F_H(\rho)$ (eV)
$\rho \leq 15$	$0.511261 - 0.199975 \times (\rho - 15)$
$15 < \rho \leq 20.2$	$0.009405 - 0.022205 \times (\rho - 20.2) - 0.000005 \times (\rho - 20.2)^2 - 0.001185 \times (\rho - 20.2)^3 + 0.000923 \times (\rho - 20.2)^4 + 0.000120 \times (\rho - 20.2)^5$
$20.2 < \rho \leq 23.7$	$0.02 \times (\rho - 23.7) - 0.004738 \times (\rho - 23.7)^3 - 0.001046 \times (\rho - 23.7)^4 - 0.000063 \times (\rho - 23.7)^5$
$23.7 < \rho$	$0.02 \times (\rho - 23.7)$

Table A2. Analytic expression for the 'interstitial' atomic electronic density, $\rho_{at}^{int}(r)$, in arbitrary units, coherent with Table A1. r is the distance from an Al particle to the position where H is embedded, in units of a_0, the lattice parameter of Al.

r (a_0)	$\rho(r)$
$r \leq 0.4$	$7.583390 - 49.822873 \times (r - 0.4) - 1489.594377 \times (r - 0.4)^2$
$0.4 < r \leq 0.7$	$105 \times \exp(-6.57 \times r)$
$0.7 < r \leq 0.9$	$-740.512898 \times (r - 0.9)^3 - 4971.220041 \times (r - 0.9)^4 - 9644.836278 \times (r - 0.9)^5$

and therefore the metals only feel the presence of H via the pair interaction. On the contrary, the potential felt by the H atoms is not a pair potential, as explained in the Effective Medium Theory (see the references in [23]), and therefore, F_{H} (the embedding function for H) cannot be linear. Modern EAM potentials have ρ_{at} functions that are relatively long range and we found that it is not possible to describe the trapping of H at a vacancy and at a surface if the variations of the density are only weakly modified by the absence of a particle. Therefore, we are forced to use another atomic density, short ranged, for calculating the embedding density for H atoms. They are called 'interstitial' atomic densities ρ_{at}^{int}. Equation (A1) is rewritten:

$$E_{pot} = \sum_{Mi} \left\{ F_I\left(\rho_{metal}\left(\vec{r_{Mi}}\right)\right) + 1/2 \sum_{j \neq Mi} V_{IJ}\left(\|\vec{r_j} - \vec{r_{Mi}}\|\right) \right\} + \sum_{Hi} \left\{ F_H\left(\rho_H\left(\vec{r_{Hi}}\right)\right) + 1/2 \sum_{j \neq Hi} V_{HiJ}\left(\|\vec{r_j} - \vec{r_{Hi}}\|\right) \right\}$$

where $\rho_{metal}(\vec{r_{Mi}}) = \sum_{Mj \neq Mi} \rho_{at}(\|\vec{r_{Mj}} - \vec{r_{Mi}}\|)$ and $\rho_H(\vec{r_{Hi}}) = \sum_{Mj \neq Mi} \rho_{at}^{int}(\|\vec{r_{Mj}} - \vec{r_{Hi}}\|)$. H–H interactions are only pair interactions (H has no contribution to F_H). M_i and M_j are metal particles labels. Hi is the label of a H particle.

The functional forms for F_H and ρ_{at}^{int} are given in the following tables and illustrated in Figure A1. Tabulated versions are given on request. The pair potentials are of the functional form $V(r) = Z/r \times \exp(-\alpha r)$. The interactions are smoothly brought to zero between r_{cut}^1 and r_{cut}^2 with a fifth order polynom that enforces continuity of the function, its first and second derivatives at r_{cut}^1 and r_{cut}^2. The values of the parameters are given in Table A3.

The quantities considered for the fitting of the potential are listed below. The numerical values given by the potential are specified in parenthesis. The preferred bulk site is the tetrahedral interstitial site (T), with an energy difference between octahedral (O) and tetrahedral (T) of $\Delta E_{O_T} = 0.147$ eV. A vacancy contains multiple trap sites: 8 tetrahedral (T_1) and 6 octahedral (O_1) sites. T_1 is the preferred position ($\Delta E_{seg}^{v} = -0.3$ eV). The centre of the vacancy is an unstable position for H. The bulk migration barrier is 0.2 eV for a jump from a T site towards an O site. Surface segregation on

Table A3. Parameters for the pair interactions.

	Al–H	H–H
Z (eV a_0)	0.1911028	0.23490
α ($1/a_0$)	0.4554222	4.4375
r^1_{cut} (a_0)	0.46	0.7
r^2_{cut} (a_0)	0.96	0.8

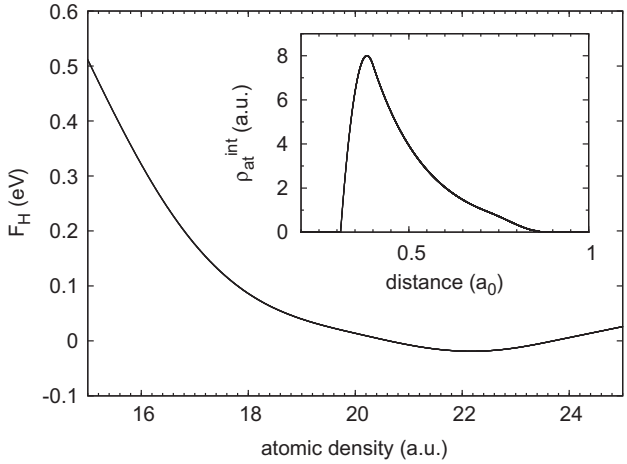

Figure A1. Embedding function F_H and atomic 'interstitial' electronic density ρ^{int}_{at} for H in Al according to the functions given in Tables A1 and A2.

the {1 1 1} surface, in the 'threefold' configuration, is −0.46 eV. In addition, a constraint to destabilize the 'on top' position is added. It is metastable with a segregation energy of +0.36 eV. The H–H repulsion is fitted to reproduce the effective pair interactions between sites 8 and 9 (30 meV) and between 9 and 10 (10 meV) of GB1.

The corresponding values given by the *ab initio* calculations from the literature are listed below. The energy difference between H in octahedral position and tetrahedral position is δE_{O-T} = +0.02 eV(+0.13 eV) [27] with (without) ZPE correction. The segregation energy in off-centred tetrahedral position in a vacancy is −0.33 eV (without ZPE) [27] and +0.46 eV in the centre of the vacancy [43]. The {1 1 1} surface segregation energy is −0.35 eV [37] and the activation energy for bulk diffusion is 0.18 eV (0.15 eV) [27].

Some additional properties of the potential are now given. A direct jump from a T site to another T site is possible, with a barrier slightly lower than T–O site (0.16 eV). The O_1 and O_2 sites (first and second octahedral interstitial neighbours of the vacancy) are unstable. Site T_2 is marginally stable, so the escape barrier from the T_1 site towards T_2 is almost equal to the opposite of the segregation energy. On the {1 1 1} surface, the bridge position is the most stable, with a segregation energy of −0.47 eV. In the case of the stable grain boundary structure, GB1, Table 1 shows that the potential is qualitatively good. It does indicate the positions where the segregation is the most favourable. The energy values do not compare quantitatively with DFT. In particular, on the most important sites (8–10) differences range between 60 and 180 meV. This EAM potential underestimates segregation to grain boundaries. Nevertheless, we will show in a forthcoming paper that a quantitative correspondence between EAM and DFT can be established and the potential used to study the impact of massive H segregation on the GB structure and cohesion, beyond mean field calculations.